Klystrons

(and other vacuum electronics power amplification devices)

Gap-Coupling, Beam-Loading Admittance

Eric Colby,

SLAC

USPAS, January 21st

Outline

- How a linac's properties interact with the power source
- General principles of microwave tubes
    - Beam loading admittance
    - Radial gap-coupling coefficient
    - Bunching
- Specific examples
- General scaling laws
- Other examples

Linac / Power Source Parameter Couplings

Linac Gradient $G' = \mathrm{sqrt}(P' \, Z'_s \, T)$

G' = gradient per unit length

P' = rf peak power per unit length

Z'_s=shunt impedance per unit length

T = transit time factor

Linac fill time $\tau = Q_L / 2\omega << \tau_{rf}$ = rf pulse length

Q_L =Accelerating loaded cavity $Q_L = Q_o/(1+\beta)$

Average Beam Power $P_b = \eta \, P_{rf}$

P_b=(average beam current) x (beam voltage gain)

η = net efficiency of coupling rf to beam

P_{rf}= rf average power ($= f^*\tau_{rf}{}^*P_{peak}$)

Linac coupling factor β = VSWR (oc) @ tube

Phase stability of linac ⇔ phase stability of source

frequency stability of source

Basic Klystron

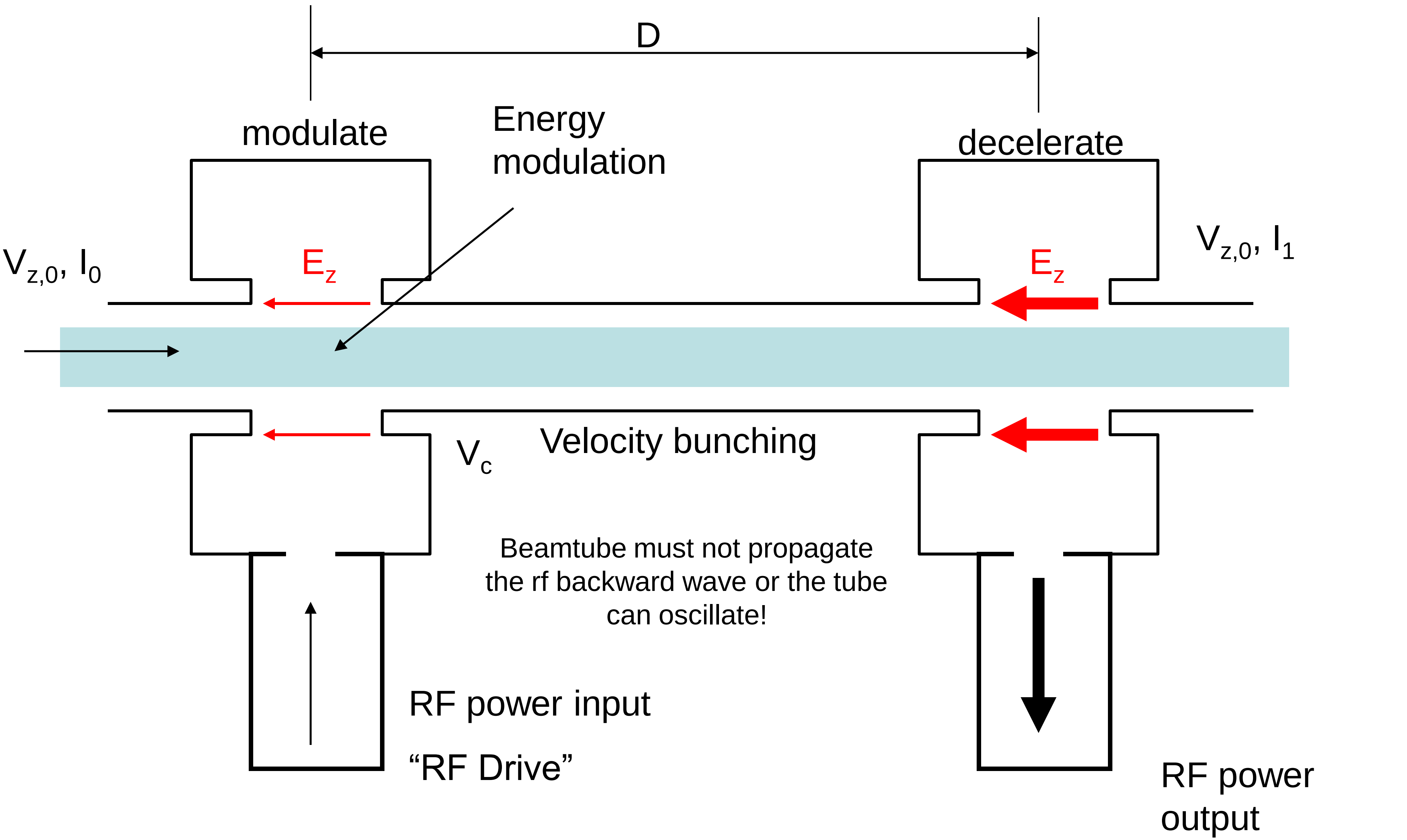

Beam Loading Admittance

So far, we've taken $\beta \rightarrow 1$ in treating beam/cavity interaction, which allows for the approximation of the beam as an ideal current source (i.e. the beam current is **not** modified by the gap voltage in the cavity).

For vacuum power tubes, however, β~(0.2-0.8) ⇔ (V=10kV-500kV), and the beam current changes significantly while *in the gap.*

$$\tilde{J}_1 = \tilde{\rho}_1 V_{z,0} + \rho_0 \tilde{V}_{z,1}$$

$$I_b = \int_S \tilde{J}_1 dS$$

0 → DC
1 → rf

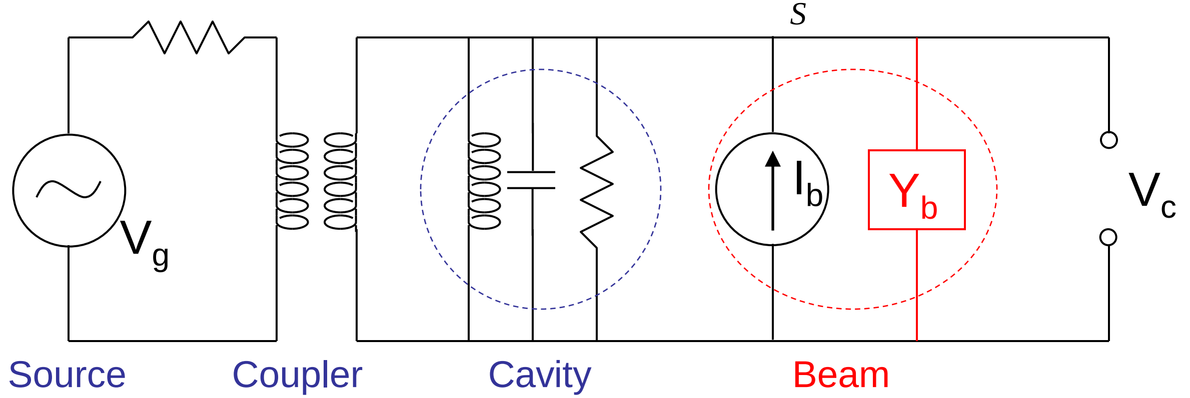

Beam Loading Admittance

Proceeding from the Continuity equation and Lorentz force law, the action of the rf fields on the beam velocity and density can be described, yielding:

$$\tilde{I}_{rf} = -I_{dc} \frac{e}{m\gamma^3 V^2{}_{z,0}} \frac{1}{j\theta} \left[1 + e^{-j\theta} + \frac{2j}{\theta}(1 - e^{-j\theta}) \right] \tilde{V}_c = \tilde{Y}_c \tilde{V}_c$$

$$writing$$

$$\tilde{Y}_c = G_c + jB_c$$

$$\theta = \frac{\omega L}{V_{z,0}}$$

Gap transit angle

Beam Loading Admittance

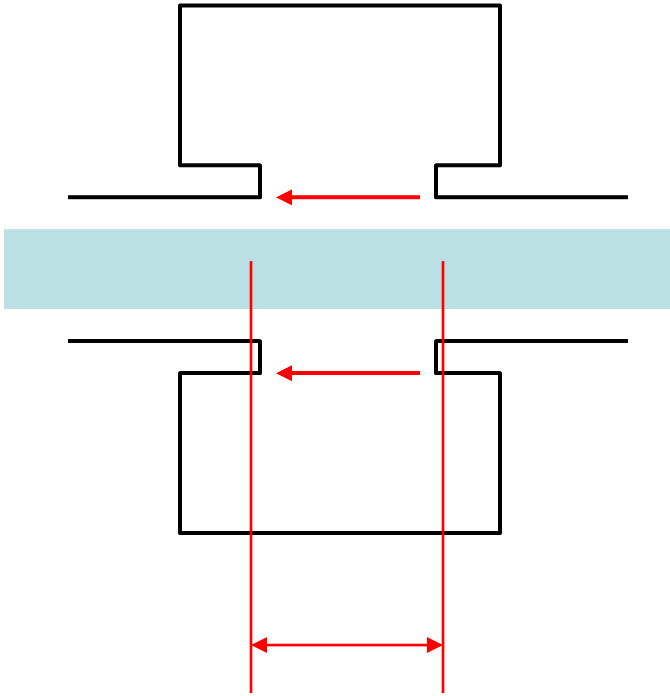

Gap length L

Gap transit angle
θ=ωL/βc

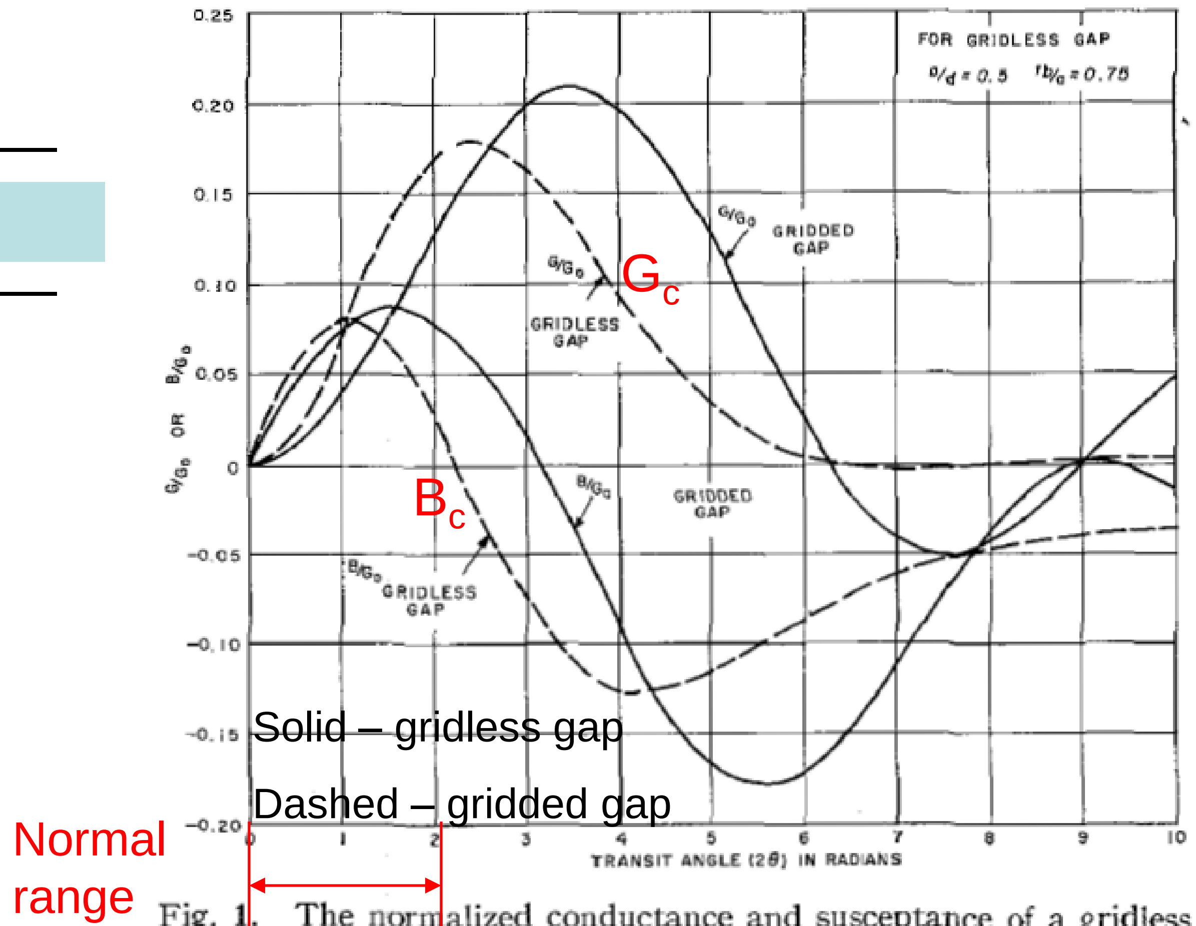

Fig. 1. The normalized conductance and susceptance of a gridless gap as a function of transit angle with $\alpha = a/d = 0.5$ and with the beam radius 75 percent of the tunnel radius. Also shown are the corresponding quantities for an ideal gridded gap which corresponds to the gridless gap with $a/d = 0$.

From E. Craig, "The Beam-Loading Admittance of Gridless Klystron Gaps", IEEE Trans. Elec. Dev. **14** (5), p. 273ff, (1967).

Gap Coupling

The beams used in vacuum tubes generally occupy a significant fracation of the beam pipe (often r_b =2/3 R_{pipe}), so the variation of the gap fields with r must be accounted for. This is done with the **radial gap coupling coefficient.**

The solution to wave equation in cylindrical coordinates yields the form of the gap voltage with r:

$$\tilde{V}_c(r,\omega) = \tilde{V}_c(R,\omega)\frac{I_0(\Gamma r)}{I_0(\Gamma R)}$$

$$\Gamma = \omega / \gamma V_z$$

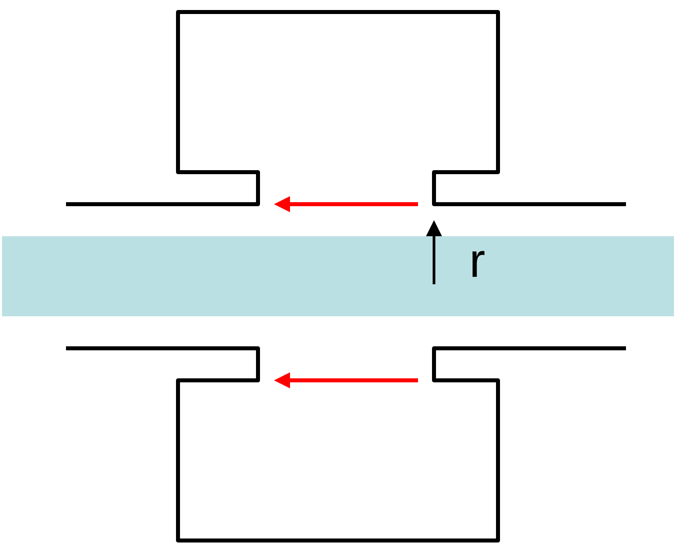

Averaging over the beam's cross section yields the gap coupling coefficient:

$$M = \frac{2I_1(\Gamma r_b)}{\Gamma r_b I_0(\Gamma R)}$$

[R/Q]→[R/Q]*M^2

Ballistic Bunching

- Ballistic (no space charge) Theory

$$I_1 = 2I_{DC} J_1(B) \exp(j(\varphi_0 - \theta_0 + \pi/2))$$

$$with$$

$$B = \frac{\theta_0}{\gamma_0^3 (V_{z,0}/c)^2} \frac{e|V_c|}{mc^2}$$ Bunching parameter

$$\theta_T = \omega D / V_{z,0}$$ Transit angle of drift D

- Matlab demonstration (space charge free)

Klystron Efficiency vs. Perveance

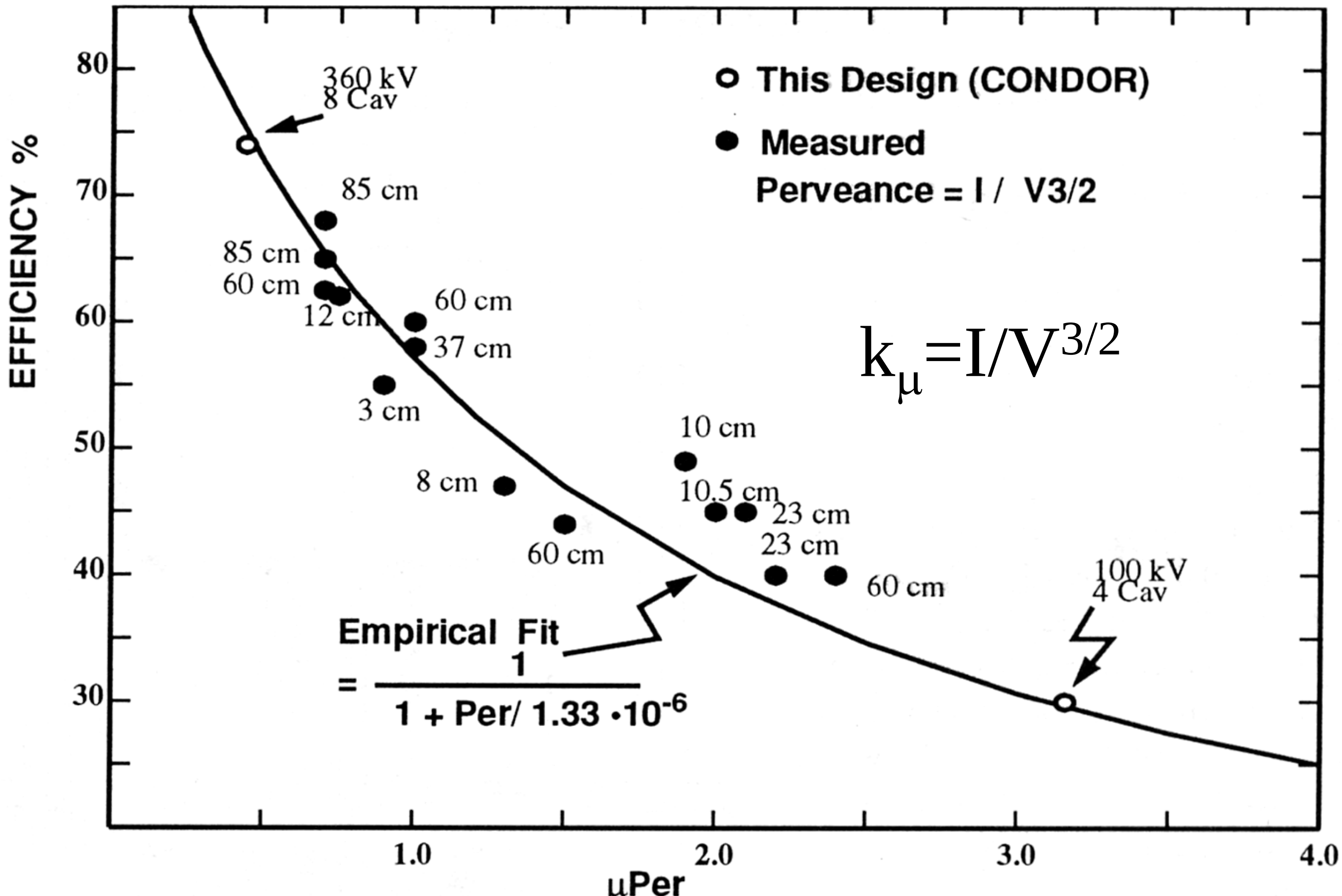

Fig. 1 The empirical relation of efficiency to the perveance.

$k_{\mu}=I/V^{3/2}$

Taken from R. Palmer, *et al*, "Status of the BNL-MIT-SLAC Cluster Klystron Project", AIP Conf. Proc. 337, p. 94ff, (1994).

Real Klystron Schematic

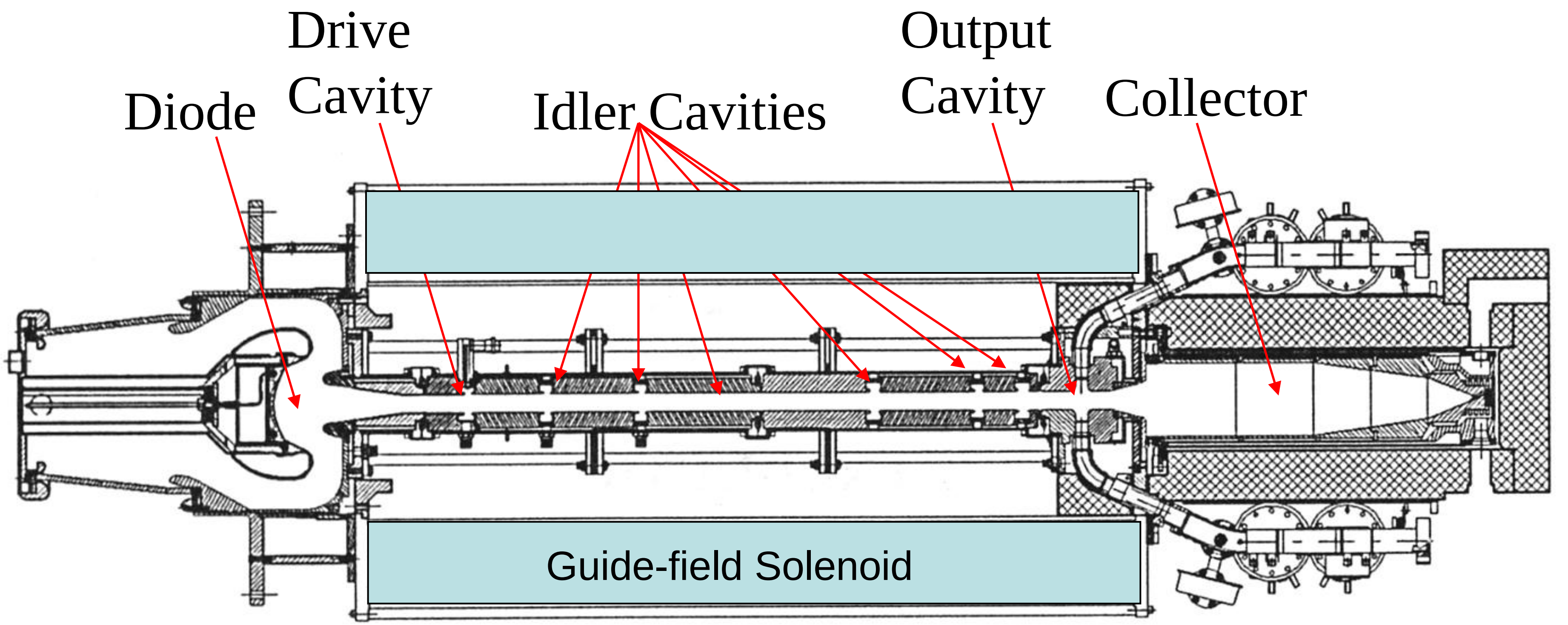

D. Sprehn, R. Phillips, G. Caryotakis, "Performance of a 150-MW S-Band Klystron", AIP Conf. Proc. 337, p.43ff, (1994).

DESY S-Band Tube (short-pulse)

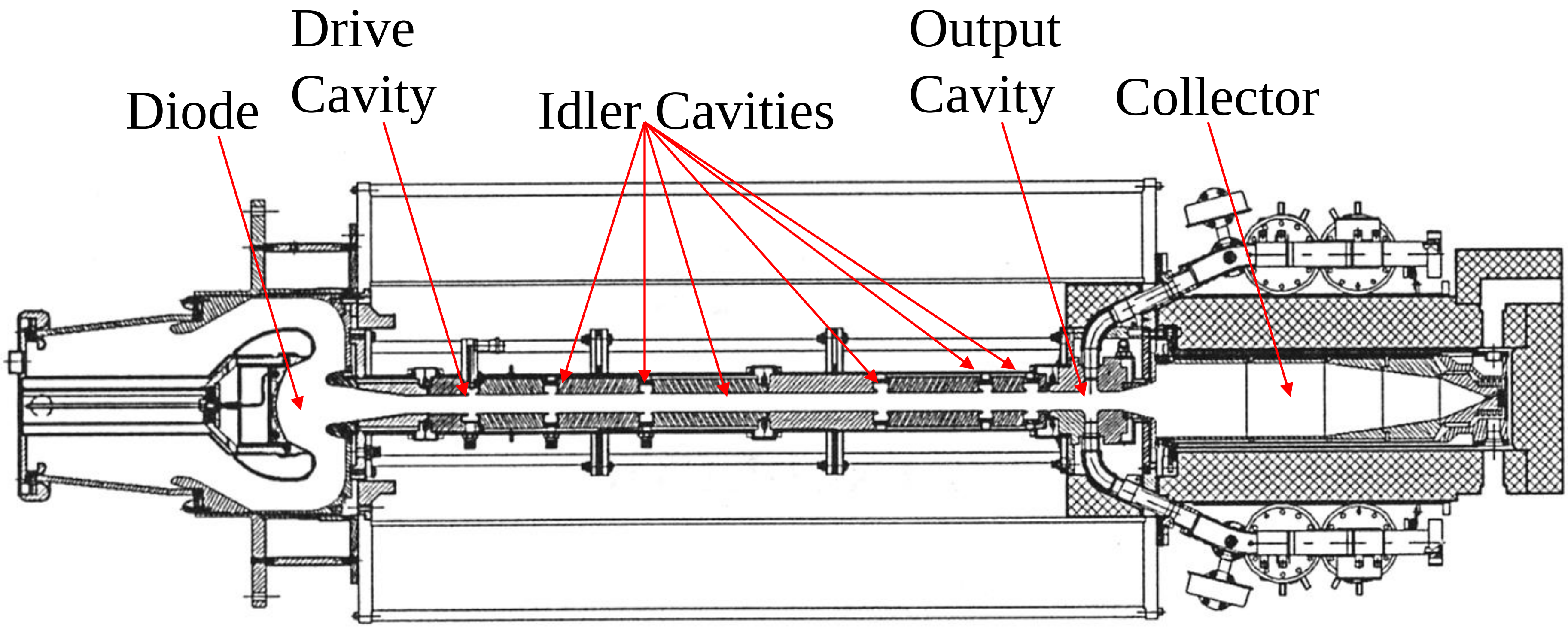

FIGURE 1. The 150-MW klystron assembly shown with magnets and lead.

f = 2996 MHz	Gain = 55 dB	Efficiency: >40%
P = 150 MW	B~2100 Gauss	PRF: 60Hz
K = 1.8 μP	Group Delay 150 nsec	Pulse length: 3 μs
V_b = 535 kV	J_{cath} = 6 A/cm^2	I_b= 700 Amps

D. Sprehn, R. Phillips, G. Caryotakis, "Performance of a 150-MW S-Band Klystron", AIP Conf. Proc. 337, p.43ff, (1994).

B-Factory Tube (CW)

f = 476 MHz	Gain > 43 dB	Efficiency: >50%
P = 1.2 MW CW	BW = +/- 3.0 MHz at -1dB points	VSWR tolerance: 1.2
K = 0.83-1.3	Group Delay 150 nsec	
V_b = 83 kV	J_{cath} = 0.63 A/cm^2	I_b= 24 Amps CW

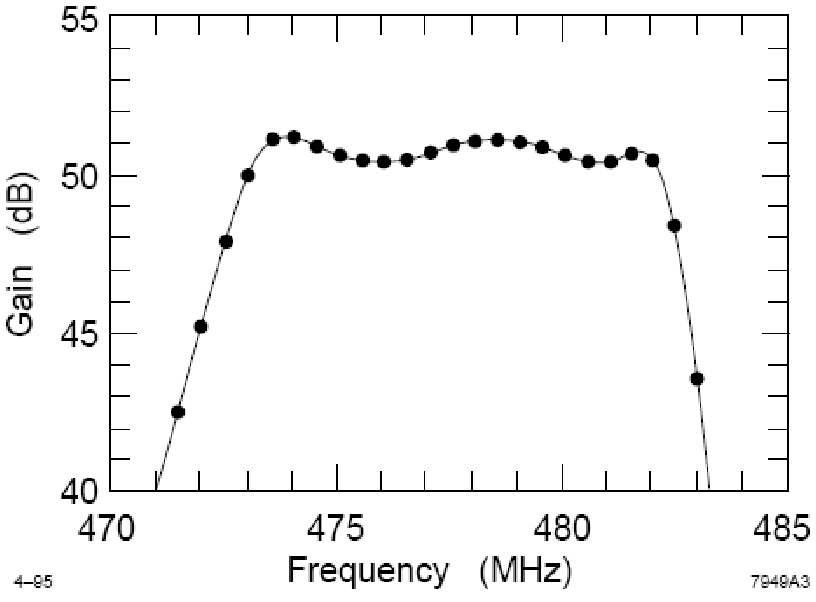

Figure 1. Predicted Small-Signal Gain versus Frequency Response at 90 KV

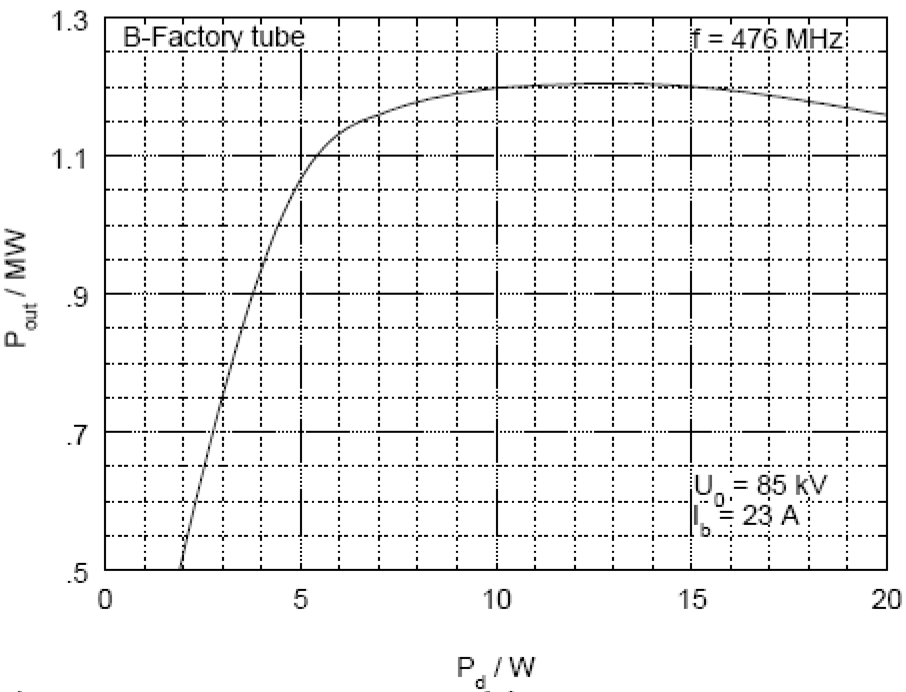

Figure 2: output power versus drive power.

Klystron Amplifier Scalings

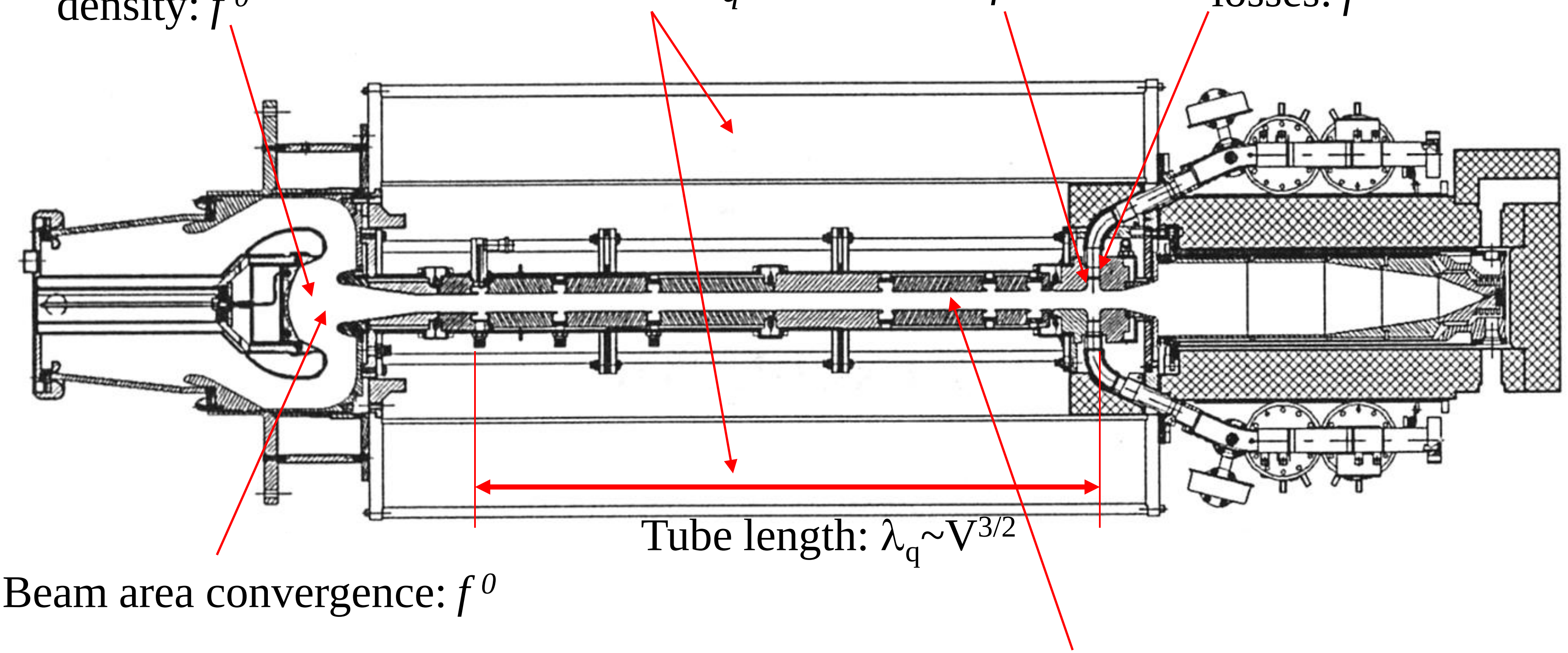

RF PULSED HEATING OF CAVITY WALLS

[O.A. Nezhevenko, PAC'97, Vancouver, 1997, p. 3013.]

Structure lifetime is limited by fatigue from pulsed heating in a thermal-diffusion layer. Assume OFE copper, NLC-like cavities, "safe" temperature excursions of 110 °C, and collider operation at 120 Hz, 6000 hrs/yr. [For 20 year life, $n = 5 \times 10^{10}$ pulses.]

[Experiments (Pritzkau, 2000) achieved $\Delta T = 120$ °C for 5.5×10^7 pulses, observed surface damage.]

CALCULATED EFFECTS OF RF PULSE HEATING OF IDEAL CAVITY WALLS.

freq ω (GHz)	$G_0 \sim \omega^{5/6}$ (MV/m)	$\tau_p \sim \omega^{-1.5}$ (ns)	$\Delta T \sim \omega^{1.42}$ (°C)	$T_o = 27$ °C		$T_o = 77$ °C	
				n	lifetime	n	lifetime
11.424	100	250	23				
22.848	180	90	61				
34.272	250	50	112				
45.696	320	30	165	3.6×10^{10}	14 yrs	2.5×10^9	1 yr
57.120	380	22	225	1.5×10^9	3500 hrs	1.8×10^8	420 hrs
68.544	440	17	290	1×10^8	230 hrs	1.8×10^7	42 hrs
79.968	500	14	370	9.8×10^6	23 hrs	2.6×10^6	6 hrs
91.392	560	11	440	1.4×10^6	3 hrs	4.7×10^5	1 hr
102.816	620	9	520	2.6×10^5	36 min	1×10^5	14 min
114.240	680	8	600	6×10^4	8 min	3×10^4	4 min

For collider applications, RF technology development >40 GHz appears unjustified

Omega-P, Inc. – Yale University
Beam Physics Collaboration

Slide courtesy of J. Hirshfield, to be published in Proc. 10th Adv. Accel. Conc. Workshop, Oxnard, CA, June 23-28 (2002).

Typical operational problems with a klystron

- Input drive power is too low and klystron is not saturated (although this is *required* if the tube is included in a feedback loop) ➔ reduced output power, efficiency, and increased output power amplitude jitter
- Wrong cathode filament current ➔ wrong perveance ➔ poor efficiency (minor) or beam interception (major)
- Modulator voltage jitter causes jitter in
  - The tube output power $P \sim V^{5/2} \rightarrow \delta P/P \sim (5/2)(\delta V/V)$
  - The tube transit time, which in turn causes phase jitter on the output $\partial\phi / \partial V = (Lf/\beta^3\gamma^3 c)$
- Mismatched load causes significant output instability

Typical Klystron Failure Modes

- Burnt-out or shorted cathode filament
- Beam interception erodes output cavity
- Rf breakdown erodes the output cavity
- Multipactoring on or near the output window sputters metal onto the ceramic window, resulting in breakdowns
- Slow vacuum leak contaminates (“poisons”) the cathode
- Focusing magnetic field changes, resulting in a current density change that either:
  - If minor: changes the gap-coupling and space charge forces
  - If major: results in beam interception
- Input cavity erodes (rare)
- Output cavity oscillates (not necessarily at an integer multiple of the rf frequency)
- Gun supports an rf resonance

Examples of other beam-based power amplifiers

17.136 GHz Klystron (Haimson Research, NRL)

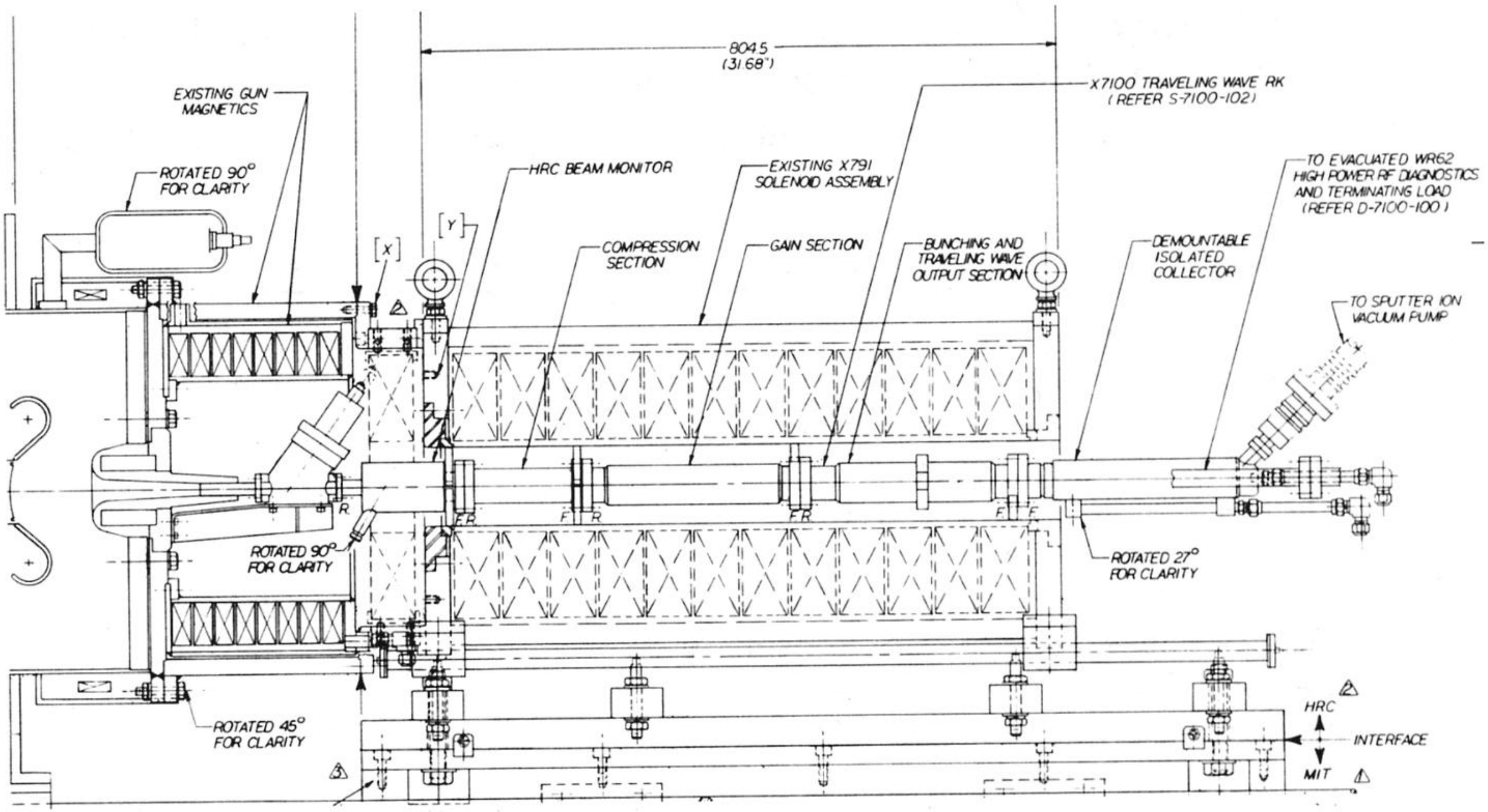

FIGURE 2. Prototype 17 GHz TWRK and solenoid assembly showing the electron gun vacuum isolation valve and the precision alignment supporting mechanism.

Taken from J. Haimson, B. Mecklenberg, B. Danly, "Initial Performance of a High Gain, High Efficiency 17 GHz Traveling Wave Relativictic Klystron for High Gradient Accelerator Research", in AIP Conf. Proc. 337, p.146ff, (1994).

17.136 GHz Klystron

(Haimson Research, NRL)

Measured Properties:

- Output Power: 26 MW @ 150 ns
- Efficiency: 49%
- Saturated Gain: 67 dB
- 560 kV/95 A beam

FIGURE 1. Model X7100 17 GHz TWRK showing the WR62 rectangular waveguide and body water-cooling connections, and the high vacuum port for the independently pumped, electrically isolated beam collector.

Taken from J. Haimson, B. Mecklenberg, B. Danly, "Initial Performance of a High Gain, High Efficiency 17 GHz Traveling Wave Relativictic Klystron for High Gradient Accelerator Research", in AIP Conf. Proc. 337, p.146ff, (1994).

1 MW, 91.4 GHz Sheet Beam Klystron (SLAC/MRC)

SBK Details:

I_o=15 A
V_o=140 kV
Perv/ □ = 14.4 nP/ □
LxW=8mm x 0.4 mm
P_{in}=400 W (at ports)
f_{rf}=91.41 GHz

PIC Details:

δt=0.135 ps=τ_{rf}/84
δz=200 μm=λ/16
N=198,000   n=17/cell
dt_{sim}/dt_{real}=3.1 ns/day

October 6, 1998

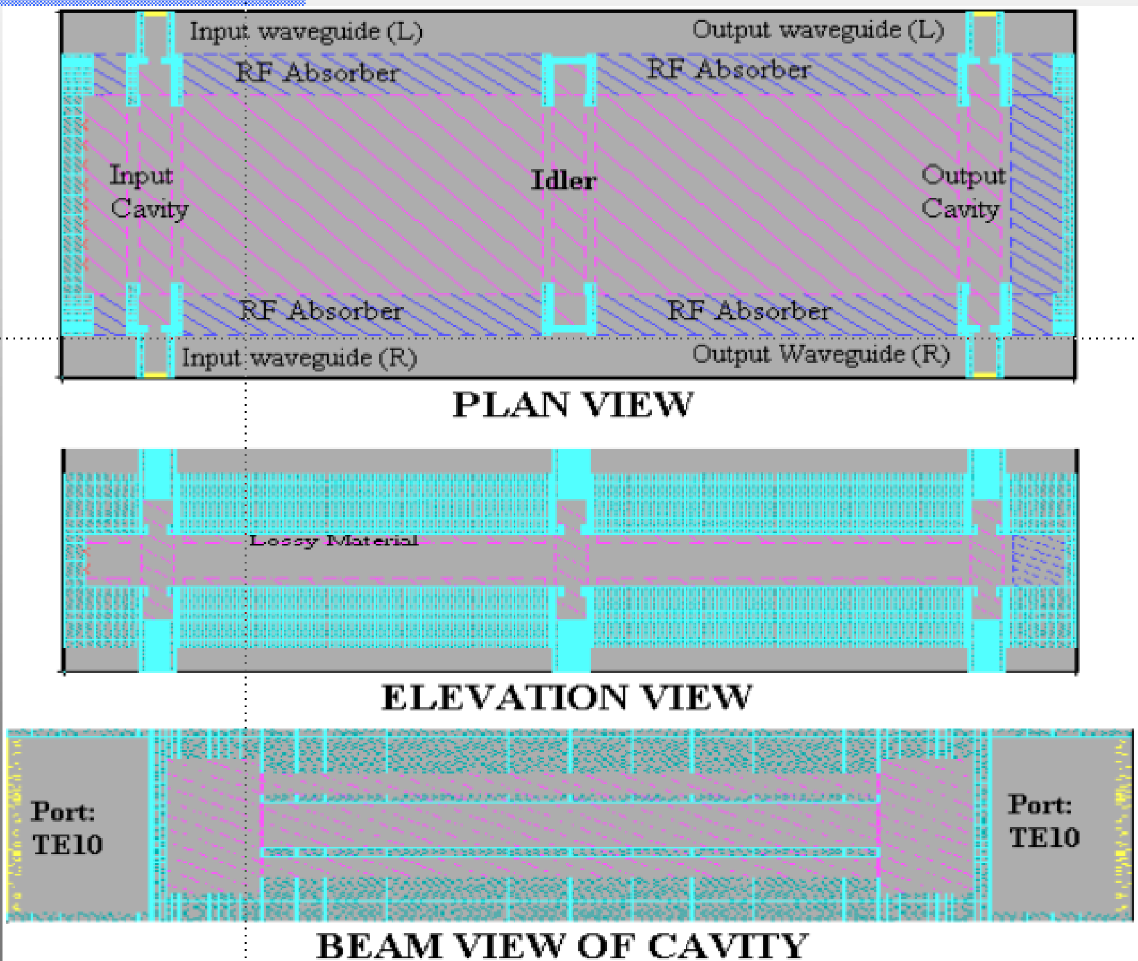

SBK Simulation

Configuration Space
Images of Bunching

Vertical Plane

Horizontal Plane

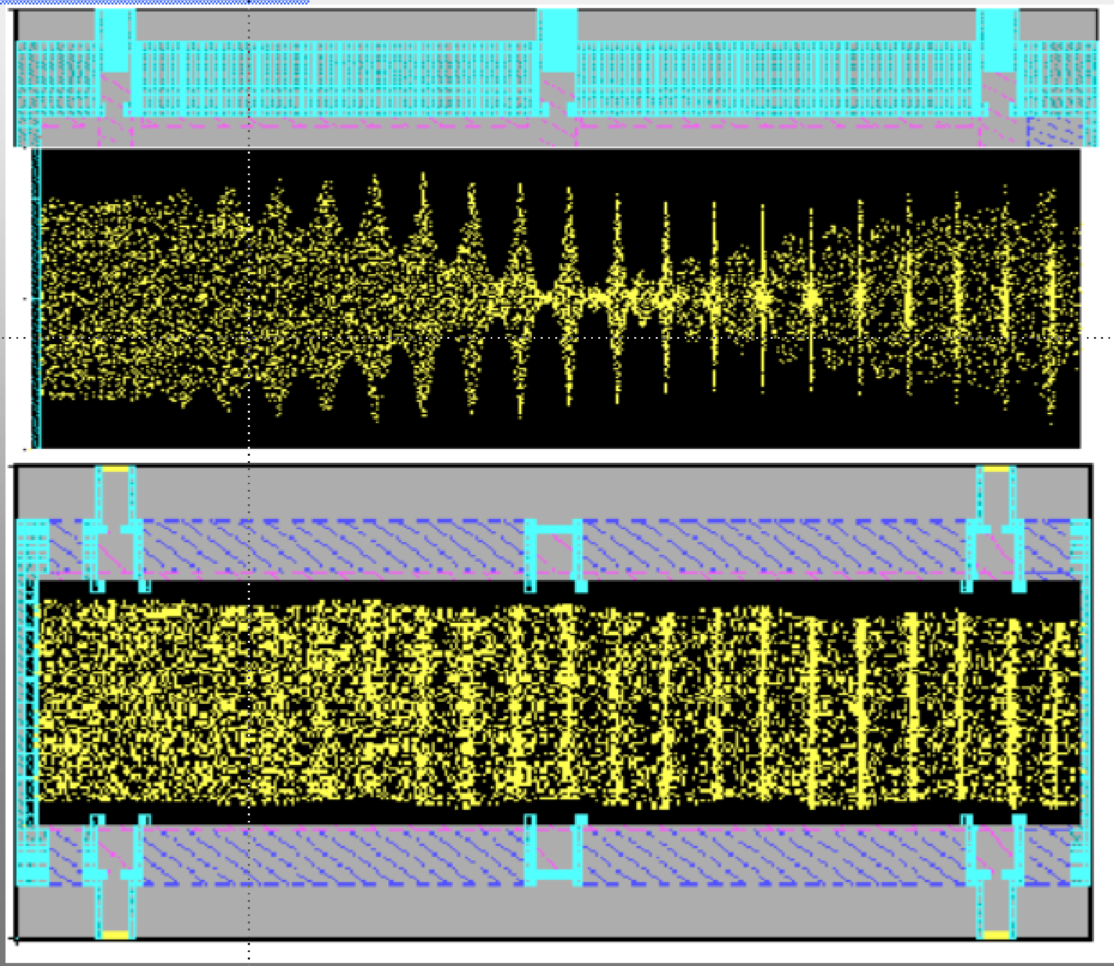

October 6, 1998

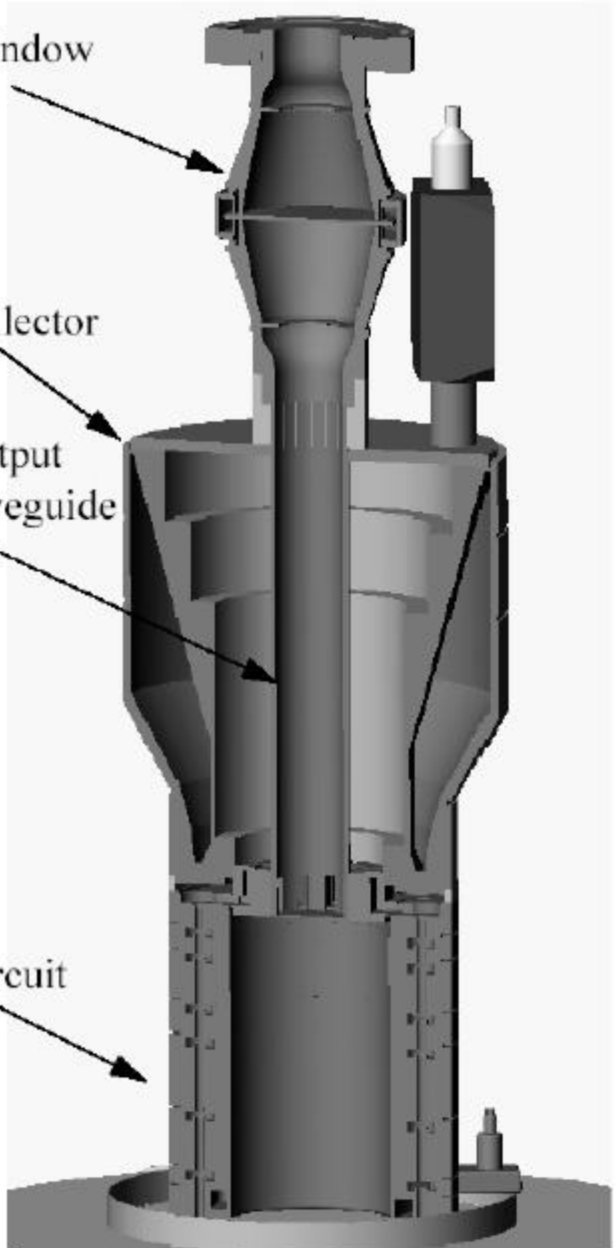

Figure 6: Cross-section of MBK

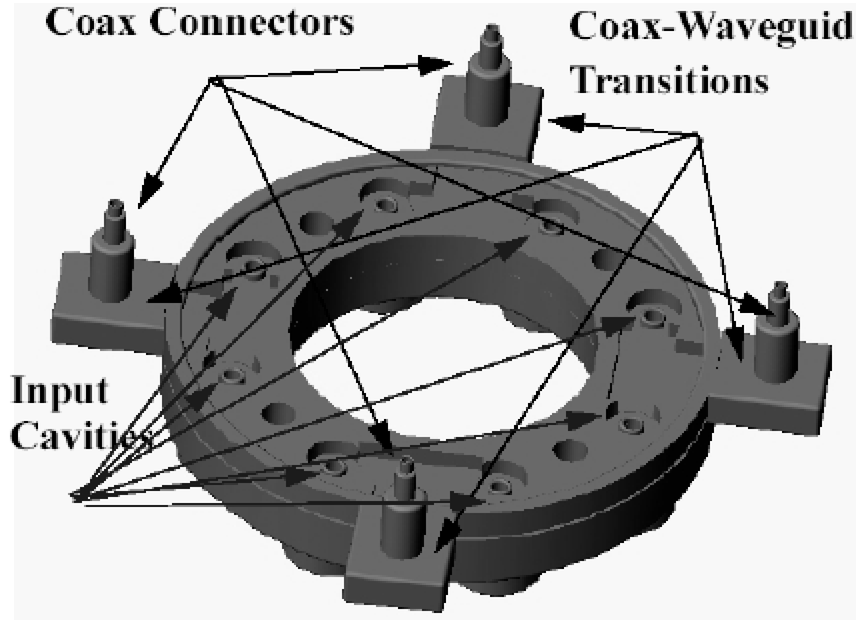

Figure 2. Input cavity assembly showing four coaxial inputs to waveguide transitions.

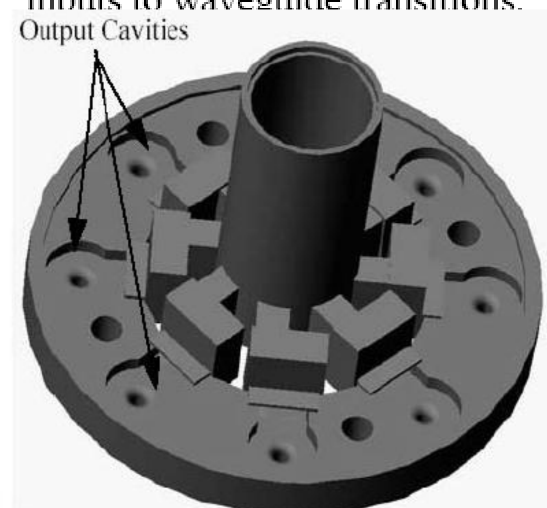

Figure 4. Output waveguide system consisting of eight waveguide twists, a TE_{01} circular waveguide, and the TE_{01} window

L. Song, *et al*, in PAC03 proc.

The Gyroklystron

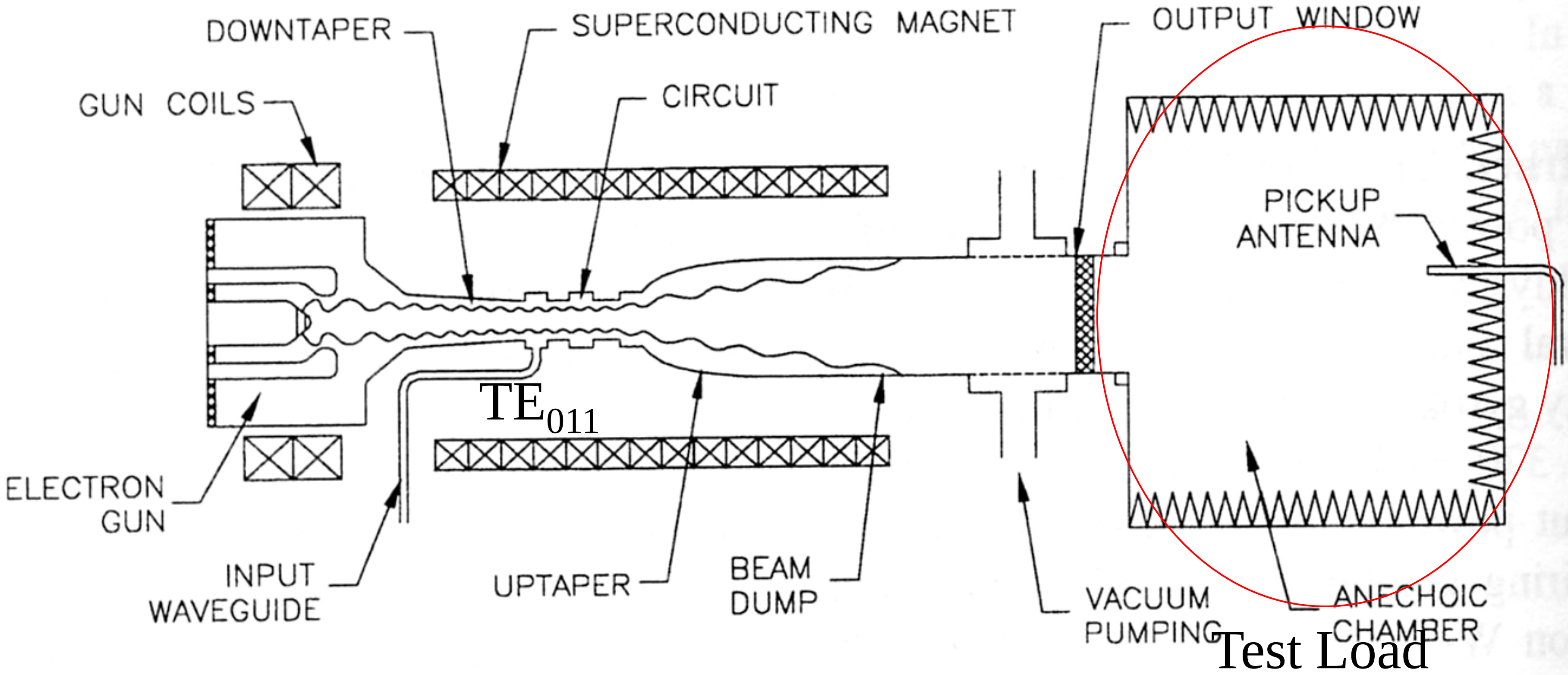

Synchronism condition: $\omega - k_{||} z_{||} = n\Omega_c$

FIGURE 1. Schematic diagram of the Ka-Band gyroklystron experiment.

Taken from M. Blank, *et al*, “Experimental Demonstration of High Power Millimeter Wave Gyro-Amplifiers”, AIP Conf. Proc. 474, p. 165ff, (1998).

Helix TWT (Preamplifier)

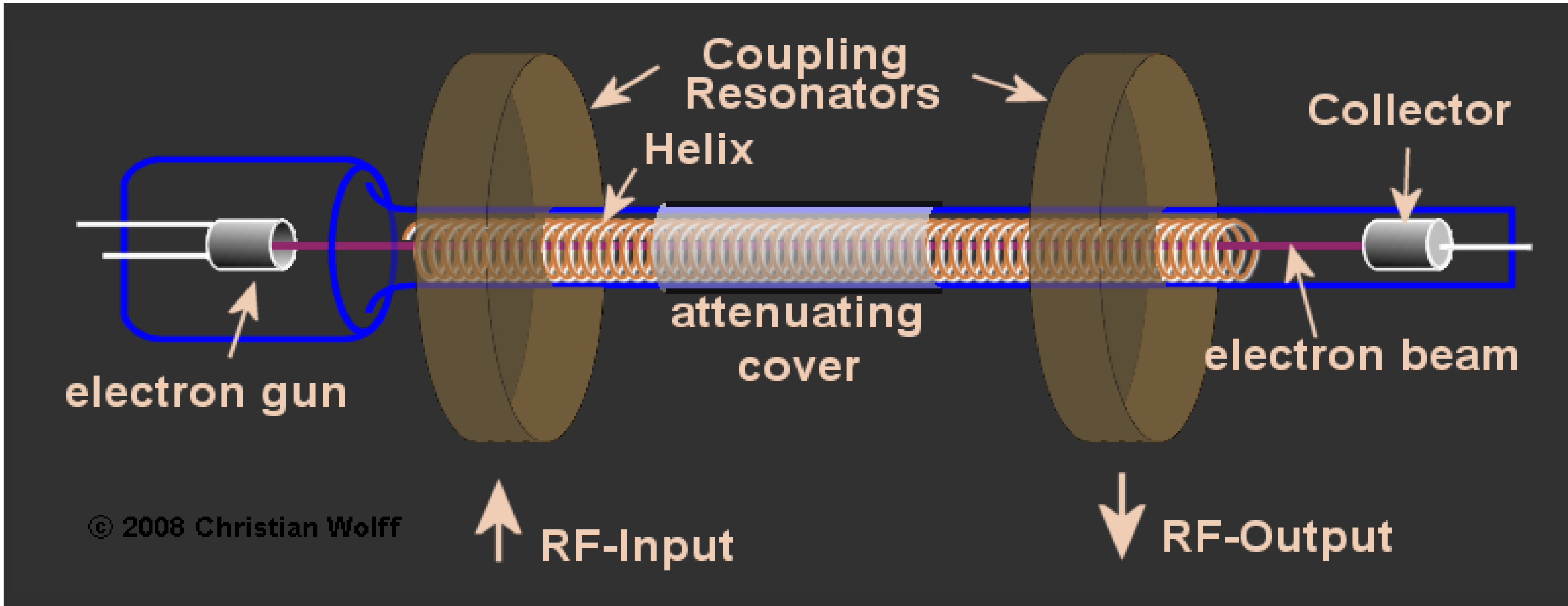

Physical construction of a traveling wave tube,

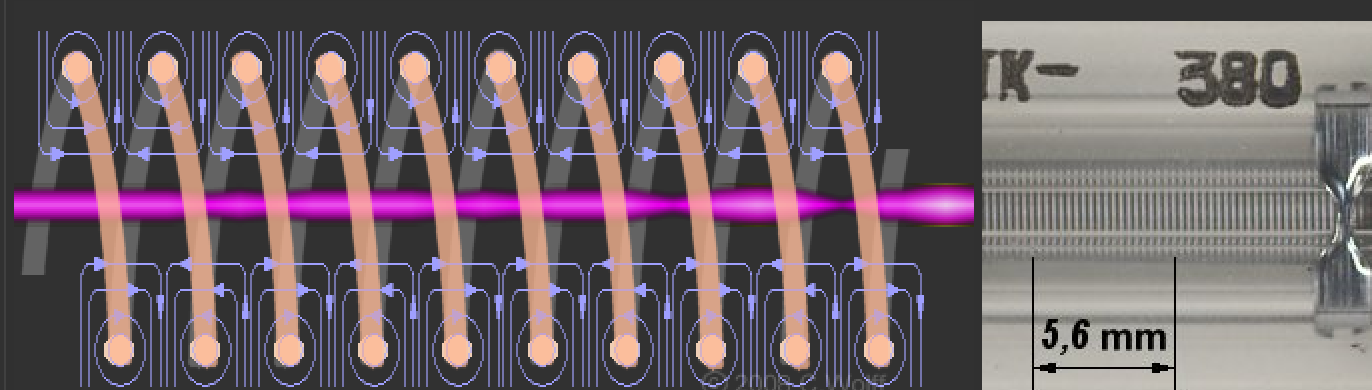

Figure 5. - electron- beam bounching and a detail-foto of a helix
(Measure detail for 20 windings)

Generally used for driving klystrons.

Gain (typ)~20-30 dB

Output~1 kW or less

34 GHz Magnicon

(Omega-P)

Energy

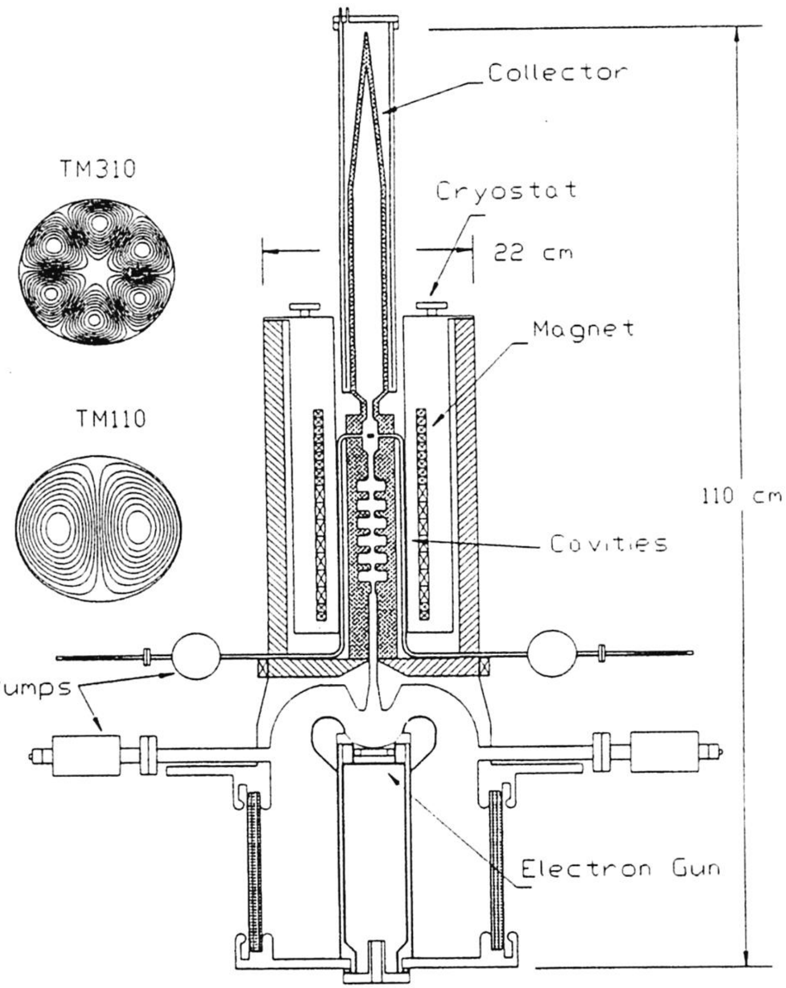

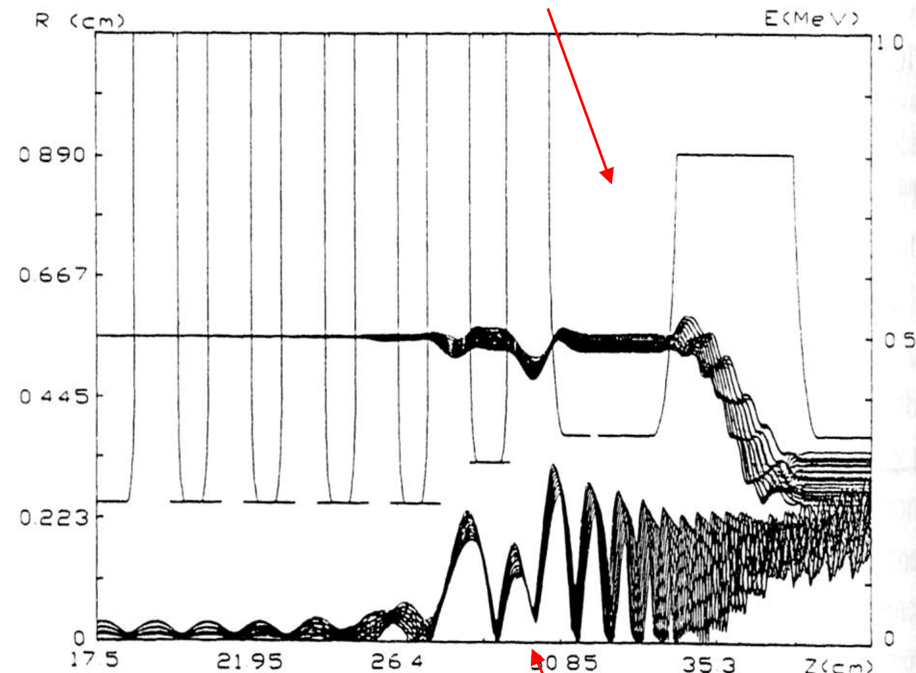

FIGURE 10. Computed steady-state evolution with z of radial orbit displacements (bottom) and partic energies (top). Also shown are the cavity outlines.

Transverse Deflection

FIGURE 1. Schematic diagram of 34.272 GHz magnicon amplifier tube. Inserts at upper left show rf field patterns for drive and all deflection cavities (TM_{110} mode at 11.424 GHz), and for the output cavity (TM_{310} mode at 34.272 GHz).

Taken from O. Nezhevenko, *et al*, "High Power Pulsed Magnicon at 34-GHz", AIP Conf. Proc. 474, p. 195ff, (1998).

Ubitron or Free Electron Laser

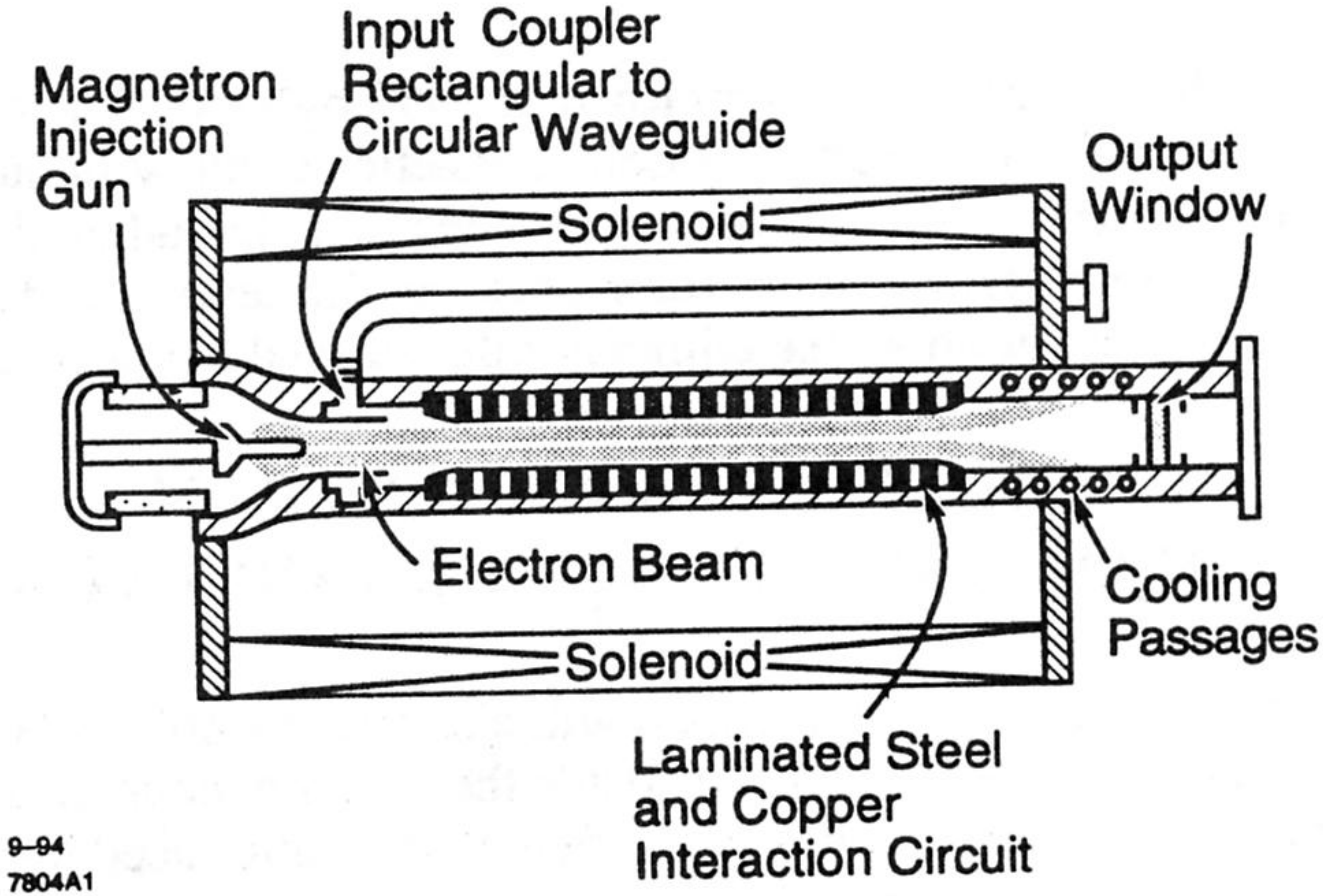

Taken from R. Phillips, “Conceptual Designs for NLC Ubitrons with Permanent-Magnet Wigglers”, AIP Conf. Proc. 317, p.239, (1994).

LLNL 140 GHz FEL Amplifier

Measured Properties:

•Power: 1-2 GW **(!)**
@ 20 ns

•Efficiency: 14%

•Beam: 6 MV/2500A

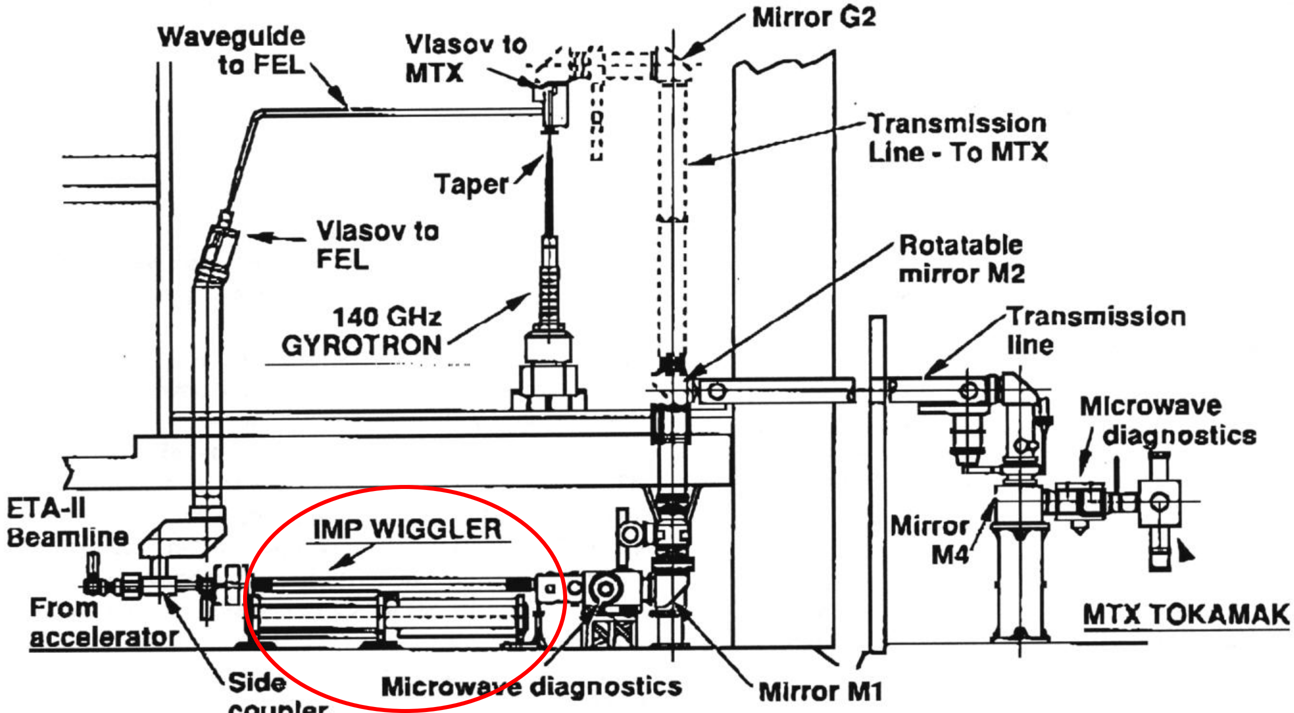

Fig. 1 The FEL is composed of the ETA-II accelerator (at left), the electron beamline, the master r (gyrotron), and the quasi-optical microwave transport system to MTX.

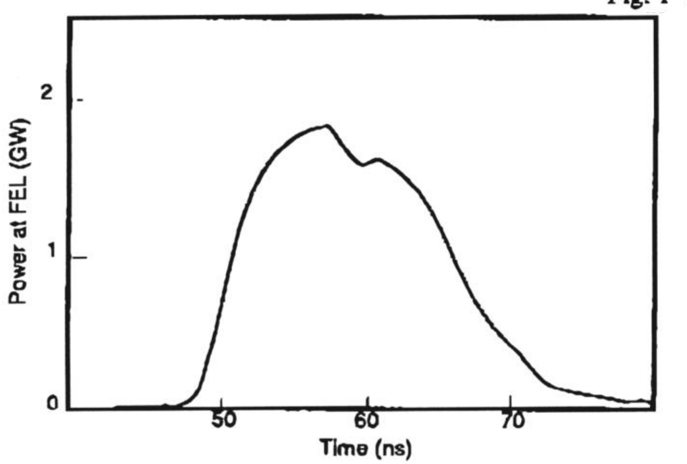

Fig. 2 A sample trace showing the output power versus time measured at the output of the FEL.

Taken from S. Allen, *et al*, “Generation of High Power 140 GHz Microwaves with an FEL for the MTX Experiment”, in Proc. IEEE Part. Accel. Conf. (PAC 93), Washington, D.C., p.1551ff, (1993).

Compact Linear Collider (International collaboration centered at CERN)

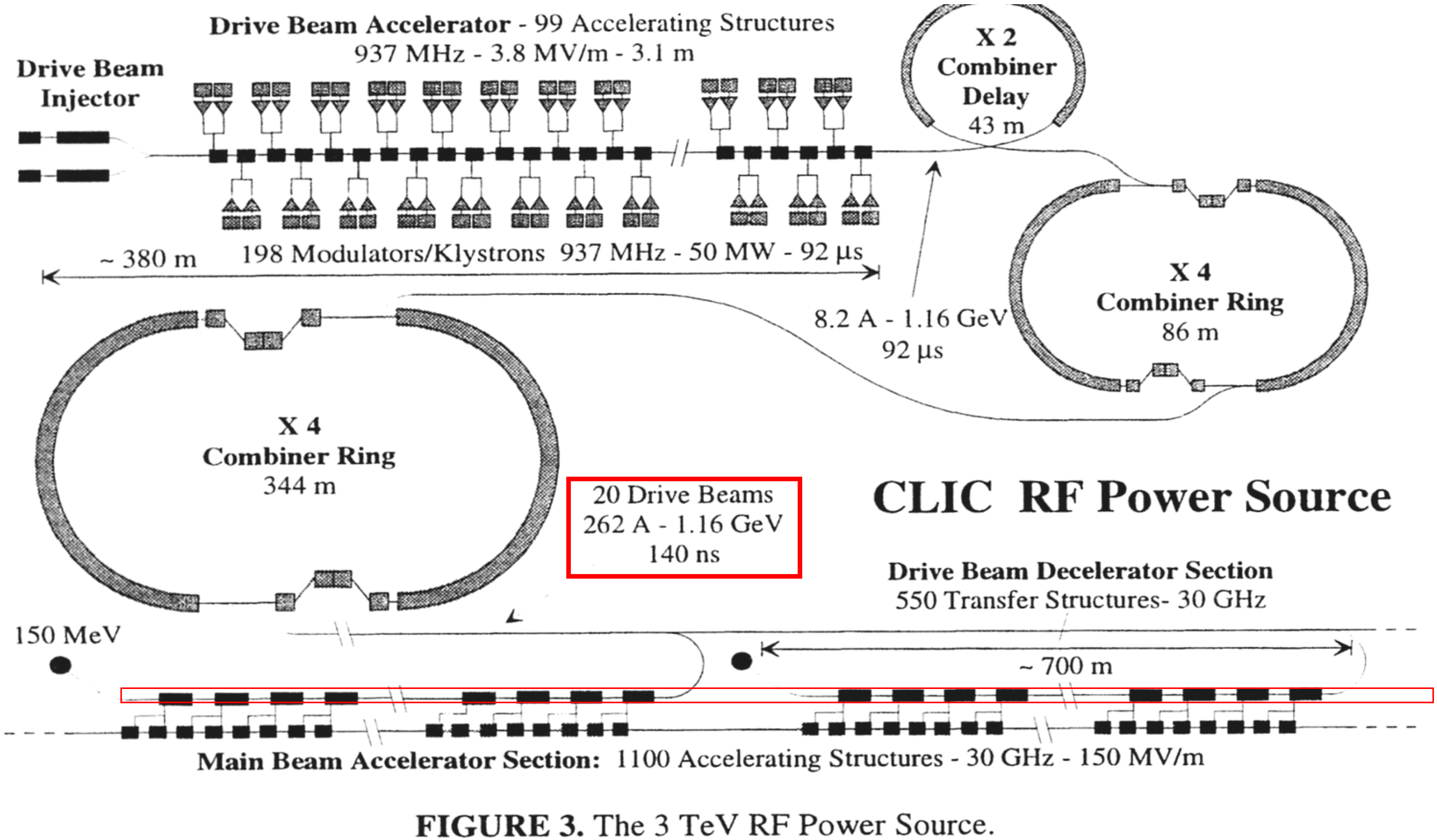

FIGURE 3. The 3 TeV RF Power Source.

Taken from H. Braun, *et al*, “A New Method for RF Power Generation for Two-Beam Linear Colliders”, AIP Conf. Proc. 474, p.1ff, (1998).

CLIC Test Facility II

Inset photo taken from H. Braun, *et al*, “A New Method for RF Power Generation for Two-Beam Linear Colliders”, AIP Conf. Proc. 474, p. 1ff (1998).

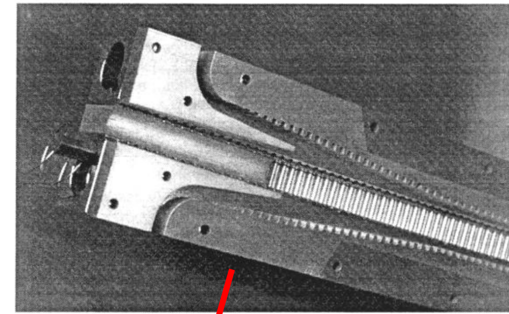

FIGURE 7. A four-channel decelerator structure.

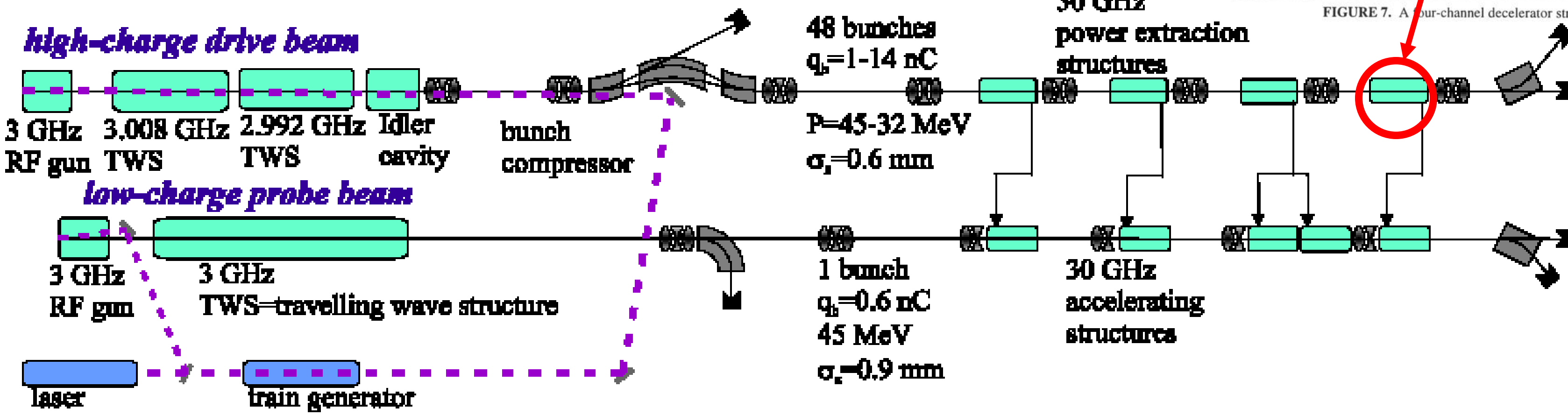

Figure 1: Configuration of CTF II during the 1999 run

Taken from: H. Braun, *et al*, “Experimental Results and Technical Research and Development at CTF II”, in Proc. Euro. Part. Accel. Conf., Vienna, Austria, p.48ff, (2000).

CTF-II Demonstrated:

- Generation and acceleration of 48x13.4 nC drive beam
- 120 MW of 30 GHz power generation in 16 ns pulses from the Power Extraction and Transfer Structures
- 59 MV/m acceleration of the probe beam

High Power Fiber Lasers

Analysis of the scalability of diffraction-limited fiber lasers and amplifiers to high average power

Jay W. Dawson, Michael J. Messerly, Raymond J. Beach, Miroslav Y. Shverdin, Eddy A. Stappaerts, Arun K. Sridharan, Paul H. Pax, John E. Heebner, Craig W. Siders and C.P.J. Barty

Lawrence Livermore National Laboratory, L-470, P.O. Box 808, Livermore, CA 94551
*Corresponding author: dawson17@llnl.gov

Abstract: We analyze the scalability of diffraction-limited fiber lasers considering thermal, non-linear, damage and pump coupling limits as well as fiber mode field diameter (MFD) restrictions. We derive new general relationships based upon practical considerations. Our analysis shows that if the fiber's MFD could be increased arbitrarily, 36 kW of power could be obtained with diffraction-limited quality from a fiber laser or amplifier. This power limit is determined by thermal and non-linear limits that combine to prevent further power scaling, irrespective of increases in mode size. However, limits to the scaling of the MFD may restrict fiber lasers to lower output powers.

OCIS codes: (140.3510) Lasers, fiber; (140.4480) Optical amplifiers

References and links

1. A. Tünnermann, T. Schreiber, F. Röser, A. Liem, S. Höfer, H. Zellmer, S. Nolte, and J. Limpert, "The renaissance and bright future of fibre lasers," J. Phys. B **38**, 681 (2005).
2. T. Simpson, F. Doft, P. Peterson, and A. Gavrielides, "Coherent combining of spectrally broadened fiber lasers," Opt. Express **15**, 11731–11740 (2007).
3. A. Shirakawa, K. Matsuo, and K. Ueda, "Fiber laser coherent array for power scaling, bandwidth narrowing, and coherent beam direction control," in Proc. of the SPIE: Fiber Lasers II: Technology, Systems, and Applications, **5709**, 165-174 (The International Society for Optical Engineering, 2005).
4. S. Chen, Y. Li, and K. Lu, "Branch arm filtered coherent combining of tunable fiber lasers," Opt. Express **13**, 7878-7883 (2005).
5. J. Boullet, D. Sabourdy, A. D. Berthelemot, V. Kermène, D. Pagnoux, P. Roy, B. Dussardier, and W. Blanc, "Coherent combining in an Yb-doped double-core fiber laser," Opt. Lett. **30**, 1962-1964 (2005).
6. J. Xu, S. Zhao, S. Zhan, R. Hou, Y. Li, L. Shi, and S. Fang, "High power high brightness laser source for material processing through incoherent beam combination," Proc. of the SPIE **6722**, 67221D-1-5 (The International Society for Optical Engineering, 2007).
7. R. K. Huang, L. J. Missaggia, J. P. Donnelly, C. T. Harris, and G. W. Turner, "High-brightness slab-coupled optical waveguide laser arrays," IEEE Photon. Tech. Lett. **17**, 959-961 (2005).
8. S. J. Augst, J. K. Ranka, T. Y. Fan, and A. Sanchez, "Beam combining of ytterbium fiber amplifiers," J. Opt. Soc. Am. B **24**, 1707-1715 (2007).
9. T. H. Loftus, A. M. Thomas, P. R. Hoffman, M. Norsen, R. Royse, A. Liu, and E. C. Honea, "Spectrally Beam - Combined Fiber Lasers for High - Average - Power Applications," IEEE J. of Sel. Top. Quantum Electron. **13**, 487–497 (2007).
10. D. Walton, S. Gray, J. Wang, M. Li, X. Chen, A. Liu, L. Zenteno, and A. Crowley, "Kilowatt - Level, Narrow - Linewidth Capable Fibers and Lasers," Proc. of SPIE **6453** (2007).
11. J. D. Hansryd, "Increase of the SBS threshold in a short highly nonlinear fiber by applying a temperature distribution," J. Lightwave Tech. **19**, 1691-1697 (2001).
12. J. C. Knight, "Photonic Crystal Fibers and Fiber Lasers," J. Opt. Soc. Am. B **24**, 1661-1668 (2007).
13. P. S. J. Russell, "Photonic-Crystal Fibers," J. Lightwave Tech. **24**, 4729-4749 (2006).
14. J. C. Baggett, T. M. Monro, K. Furusawa, and D. J. Richardson, "Comparative study of large-mode holey and conventional fibers," Opt. Lett. **26**, 1045-1047 (2001).
15. Y. Jeong, J. Sahu, D. Payne, and J. Nilsson, "Ytterbium-doped large-core fiber laser with 1.36 kW continuous-wave output power," Opt. Express **12**, 6088-6092 (2004).

#97711 - $15.00 USD Received 20 Jun 2008; revised 1 Aug 2008; accepted 3 Aug 2008; published 13 Aug 2008

18 August 2008 / Vol. 16, No. 17 / OPTICS EXPRESS 13240

IPG PHOTONICS The Power to Transform™

Typical Specifications

Optical Parameters

	Unit	YLR-1000*	YLR-3000	YLR-5000	YLR-10000	YLR-20000
Nominal Output Power	W	1000	3000	5000	10000	20000
BPP after Feeding Fiber	mm*mrad	<2.0*	<2.0	<4.0	<5	<12
BPP after Processing Fiber	mm*mrad	<4	<4	6	<8	-
Feeding Fiber Core Diameter	um	50	50	100	100	200
Processing Fiber Core Diameter	um	100	100	150	200	-

Electrical Parameters

	Unit	YLR-1000	YLR-3000	YLR-5000	YLR-10000	YLR-20000
Electrical Requirements	V AC	360-528V, 3P+PE, 50-60Hz				
Typical Power Consumption	kW	3.5-4	10-12	17-20	35-40	70-80
Standard Interfaces		Ethernet, Digital I/O, Analog, PROFIBUS**, DeviceNet**				
Direct Modulation	kHz	0-5	0-5	0-5	0-5	0-5

General Parameters

	Unit	YLR-1000	YLR-3000	YLR-5000	YLR-10000	YLR-20000
Max. Cooling Water Consumption (25ºC)	m³/h	0.6	1.4	2.5	4	7
Cooling Water Temperature Range	ºC	20-25	20-25	20-25	20-25	20-25
Dimensions (W x H x D)	cm	86x120x81	86x120x81	110x150x81	110x150x81	210x150x81
Weight	kg	250	350	500	750	1200
Ambient Temperature	ºC	10-50	10-50	10-50	10-50	10-50
Enclosure Type		IP-54	IP-54	IP-54	IP-54	IP-54

* - 1 and 2kW lasers also available in with a single mode output versions YLR-1000-SM and YLR-2000-SM respectively. In this case BPP is ~0.4 mm * mrad from a 20um feeding fiber and ~2 mm*mrad from a 50um processing fiber. All other electrical and general parameters are the same as for YLR-1000 and YLR-2000 lasers.

** - optional, on request.

http://www.ipgphotonics.com/documents/documents/HP_Broshure.pdf

Carrier Phase-Locked Lasers

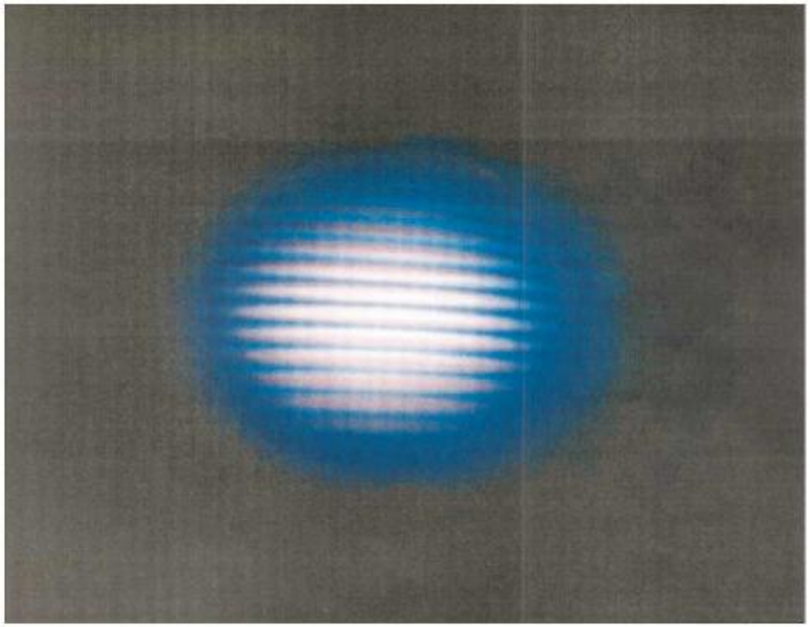

Fig. 2. White-light fringes resulting from the interference of the two continua generated by the two phase-locked IR laser pulses when the relative delay is properly adjusted to zero.

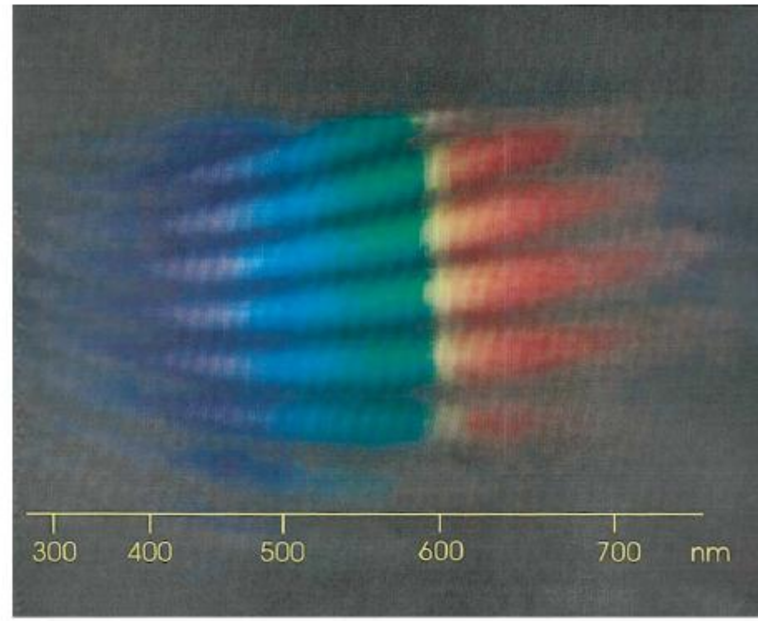

Fig. 3. Spectrally dispersed white-light fringes. Clear and well-defined fringes indicate that a stable phase relationship is conserved across all the generated visible spectrum.

Interference fringes of carrier phase-locked white light continua generated from Ti:Sapphire laser.

M. Bellini, T Hansch, Optics Letters, **25** (14), p.1049, (2000).

Sources by Power Density and Wavelength